Particle-based modeling of hypervelocity impact and fragmentation in materials

Martin Oliver Steinhauser[1,2,3]

[1] Fraunhofer-Institute for High-Speed Dynamics, Ernst-Mach-Institut, Ernst-Zermelo-Strasse 4, Freiburg, Germany, martin.steinhauser@emi.fraunhofer.de
[2] Department of Chemistry, University of Basel, Klingelbergstrasse 80, CH-4056, Switzerland, martin.steinhauser@unibas.ch
[3] Fraunhofer Singapore, 50 Nanyang Avenue, Block N51-1, Nanyang Technological University, Singapore 639798 martin.steinhauser@fraunhofer.sg

ABSTRACT

Numerical simulations of hypervelocity impact (HVI) phenomena are an important part of hypervelocity research, but also face challenges due to the large deformations and shock wave discontinuities involved. The most common methods currently used for such simulations are meshless particle-based methods, such as Smoothed Particle Hydrodynamics (SPH), which can handle the large deformations and creation of new free surfaces caused by fragmentation and spallation. Other techniques include hybrid methods which combine particle methods with mesh based finite element formulations. All of these numerical methods have been shown to perform and represent HVI phenomena relatively well, but they are based on continuum theory which is not ideally suited for modeling fracture and failure in materials and for representing the discontinuities in shock waves responsible for many HVI phenomena. In this paper we present a completely different approach to simulating HVI by using a discrete method. We focus our numerical investigations on the dynamics of the material fragmentation upon impact with the goal of demonstrating the feasibility of using a discrete approach for simulating HVI phenomena. The simulation model we present in this paper is loosely based on the Discrete Element Method (DEM). For modeling the solids, we use discrete spherical particles interacting with each other via potentials. The particles are linked together via spring potentials to form a solid. Fracture and fragmentation are handled by removing the springs connecting individual particles. The parameters for the model were chosen by direct comparison to HVI experiments performed at the Ernst-Mach-Institute. The focus of our numerical simulations is on HVI of thin plates and we compare our results with experimental results published in literature at a variety of impact velocities and target thickness to impactor diameter ratios. We find that our simulations correspond very well to experimental data when the impact conditions create shock pressures in the target and impactor many times greater than the material strength, but deviate when shock pressures are low. In conclusion, we examine the feasibility of using a completely discrete approach to simulate HVI phenomena. We have found that using a particle simulation method leads to very stable, energy-conserving simulations of HVI that correspond to experiments.

1 INTRODUCTION

There have only been man-made objects in space since the start of the Space Age with the launch of Sputnik on October 4, 1957. All of these objects resulted from the roughly 5.000 to 6.000 launches since then and they are commonly referred to as space debris. In the Lower Earth Orbit (LEO), this debris is more significant than natural meteoroids, and collisions in space have become a real problem that is getting an increased amount of attention. At typical collision speeds of 10 km/s, impacts by millimeter-sized objects could cause local damage or disable an operating satellite. Collisions with debris larger than 1 cm could cause the break-up of a satellite or rocket body. Finally, impact by debris larger than about 10 cm is likely to lead to catastrophic failure, i.e. the complete destruction of a spacecraft and generation of a debris cloud.

One major source of information on space debris is the US Space Surveillance Network (SSN). SSN is tracking, corelating and cataloguing more than 20.000 space objects larger than 5-10 cm in Earth orbit and it is estimated that there are more than 29.000 objects larger than 10 cm, 750.000 from 1 to 10 cm, and more than 166 million objects from 1 mm to 1 cm. Major contributions to the population of fragments came from a Chinese anti-satellite test, targeting the Feng Yun-1C weather satellite on January 11, 2007, which created more than 3.400 tracked fragments, and the approximately 2.300 tracked fragments from the first-ever accidental collision between two satellites, an active US commercial communications satellite Iridium-33, and a defunct Russian military communications satellite

Cosmos-2251, on February 10, 2009. Breaking the space debris population down by mass, Russia is responsible for roughly 40% of space junk, followed by the US (30%), China (20%) and the rest of the world (10%).

With the number of in-orbit collisions rising, a better understanding of the physics of the structural destruction and fragment generation is required as input to environment modelling. Modern methods of computational physics [1,2] are required for this purpose.

2 SIMULATION MODEL

In our simulations, we aim at modelling the dynamics of impact failure and fracture behavior of the material as observed in HVI experiments. For simplicity, we use monodisperse spheres as basic discrete elements and adjust their interactions using attractive and repulsive potentials. It has been shown that the physical observables determined by such models for granular matter depend mainly on the interaction potentials and much less on the shape of the elements used for the discretization [3, 4].

A general principle used to develop our coarse-grained model is to begin with the simplest possible working model before adding more complexity. This simplifies the investigation of the complex interactions between material parameters. Three parameters appear to be sufficient for reproducing the essential basic material properties that are important in an HVI setting where details of material strength can be simplified due to the overwhelmingly large shock pressures experienced in the case of HVI. The essential properties are: first, the resistance to pressure, second, the cohesive forces that keep the particles together to form a solid, and finally the failure on the microscopic scale.

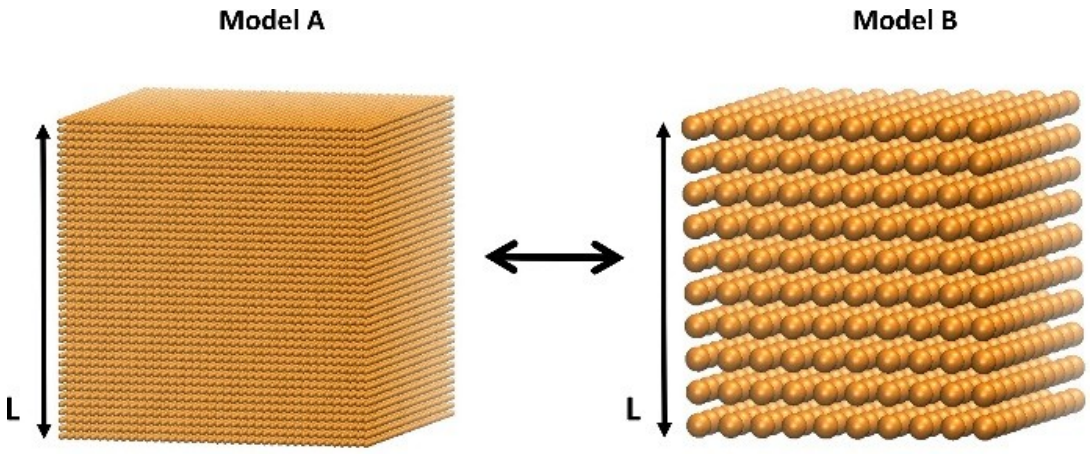

Fig. 1. Particles are initiated into a regular cubic lattice. In our model, the particle properties are independent of the number of particles, i.e. we are implementing a multiscale model.

Particle interactions can be classified as contact and bonded interactions. Bonded interactions correspond to the pairwise interactions of particles connected by a spring. Contact interactions are experienced by particles whose centers are less than two radius lengths away from each other. We do not consider shear or tangential potentials in this basic model.

2.1 Initial Setup

The particles are initiated into a regular cubic lattice structure, as seen in Fig.1. Each particle has two properties: mass m_i, and a length scale, diameter a_i, according to the system's geometry. In the simulations presented here, we chose a monodisperse configurations of particles, i.e., all masses $m_i = m$ and all lengths scales $a_i = a$ are the same for all particles. To form larger solids, many particles are connected with massless spring, also referred to as bonds. Then, a small random velocity taken from an equilibrium Boltzmann-distribution is applied to each particle. This random velocity ensures that the load transfer path is distributed through the material by disrupting the perfect alignments of the initial setup.

2.2 Particle Potentials

Newton's second law is used to evaluate the accelerations acting on each particle at every time step during the simulation; hence, it governs the dynamics of our model:

$$-\nabla_{ri}\Phi_{tot} = F_i = m\ddot{r}_i \tag{1}$$

with Φ_{tot} being the interaction potential, i.e. the sum of all potentials acting on each particle *i* introduced in the next section. The accelerations can then be integrated to yield velocities and positions. The forces acting on each particle are defined via pair potentials. F_i comprises the force acting on the *i*-th particle due to the interaction potentials and *m* is the mass of one particle.

2.2.1 Contact Potentials

The Lennard-Jones potential

$$\phi_{rep}{}^{LJ}(r_{ij}) = \varepsilon\left\{\left(\frac{\sigma}{r_{ij}}\right)^{12} - \left(\frac{\sigma}{r_{ij}}\right)^{6}\right\} \tag{2}$$

is a simple potential most commonly used in molecular dynamics simulations to model soft spheres [1,2,5], where $\mathbf{a}$ is the diameter of each simulation particle, $\mathbf{r_{ij}} = |\mathbf{r_j} - \mathbf{r_i}|$ is the distance between two particles, and $\boldsymbol{\varepsilon}$ is a pre–factor which has units of energy. The spheres are allowed to interpenetrate each other to a small extent (soft spheres), but quickly experience a strong repulsive potential according to $(\sigma/r_{ij})^{12}$. Beyond the particle diameter, there is a long range attractive component proportional to $(\sigma/r_{ij})^{6}$ The potential reaches a minimum value at $r_{ij} = r_{min} = 2^{1/6}\sigma \approx 1.1225\sigma$, which defines the equilibrium distance.

In the presented model, the Lennard-Jones potential is modified slightly to refine the description of the physics of particle interactions: A cutoff distance, set to the potential minimum, is defined to remove the attractive component. Beyond this distance, the potential is defined to be zero. Shortening the potential's range also provides the benefit of reducing the computational time because each particle interacts with fewer neighboring particles, which reduces the complexity of the interaction search algorithm. Additionally, the potential is shifted upwards by the factor $\boldsymbol{\varepsilon}$ to ensure smooth continuity with the spring potential such that:

$$\phi_{rep}(r_{ij}) = \begin{cases} \varepsilon\left[\left(\frac{\sigma}{r_{ij}}\right)^{12} - \left(\frac{\sigma}{r_{ij}}\right)^{6}\right] & \text{if } r_{ij} < r_{eq} \\ 0 & \text{otherwise} \end{cases} \tag{3}$$

2.2.1 Bonded Potentials

Neighboring particles are linked together to form a crystalline lattice structure. The bonded particle pairs can experience both cohesive and repulsive forces. A quadratic spring potential

$$\phi_{coh}(r_{ij}) = \begin{cases} 1/2\,\kappa(r_{ij} - r_{eq})^2 & \text{for } r_{ij} > r_{eq} \\ 0 & \text{otherwise} \end{cases} \tag{4}$$

is used for the cohesive component, and the potential of Eq. (3) for the repulsive component. Parameter $\boldsymbol{\kappa}$ is in essence the spring constant and has units of energy/length^2. The equilibrium distance $r_{eq} = 2^{1/6}\sigma$ is set to coincide with the zero-force distance of the potential of Eq. (3). In Fig. 2 we display the various potential contributions to the total interaction potential for a particle pair. The modified Lennard--Jones potential is shown in blue, with the cut-

off tail shown as a dotted line. The quadratic bonded potential is shown in red color. The distance at which the spring elements fail, r_{cut} is marked by the vertical dotted black line.

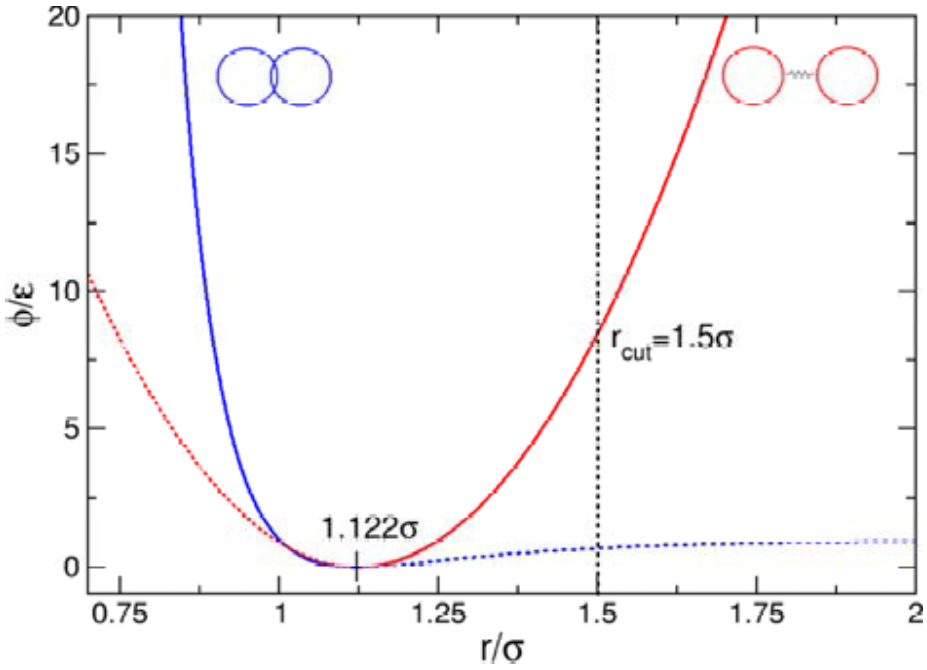

Fig 2. Repulsive (solid blue line) and cohesive (solid red line) potentials used in the model. The combined blue and red solid lines govern the forces acting on each particle pair; the dotted lines are excluded.

With the three material parameters ε, K, and r_{cut} we have developed a simple model with a minimal number of parameters with the goal of exploring the potential of DEM for HVI simulation. The essential parameters are ε representing resistance to pressure, K representing cohesive forces, and r_{cut} representing microscopic failure.

3 RESULTS AND DISCUSSION

Most of the data available for analyzing materials fragmentation and failure upon high-speed impact are high-speed photographs. Such photographs provide important information on the expansion behavior of the resulting ejecta clouds, i.e. its dimension and propagation velocity. Cloud characteristics related to fragment size distribution and the evolving structure of the cloud provide a qualitative rather than quantitative analysis from optical high-speed visualization. However, quantitative information on hypervelocity fragmentation is needed to validate new numerical methods and applications. This is considered particularly important for DEM, as the interaction behavior of the particles needs to be calibrated by appropriate test data.

The three free parameters of our model are empirically fit by comparing the simulation results directly to a recent experiment involving aluminum spheres impacting aluminum plates. We used an experiment previously performed at our institute with an impact velocity v_0 = 6.5 km/s and a ratio of plate thickness to projectile length $D/l = 0.41$. Figure 3 shows a high-speed image of the experiment with the image's intensity inverted to allow for better viewing. Due to the challenges in performing HVI experiments, multiple experiments with the exact same parameters were unavailable. The experiment shown in Fig. 3 was taken from a series of experiments studying the scalability of HVI, all of which had the same cloud expansion properties. This gives us some degree of confidence that the values measured from this single experiment are representative of HVI phenomena and therefore valid for fitting our model's parameters.

3.1 Validation with Experiments

We perform numerous HVI simulations at a variety of different impact velocities and *t/D* ratios and compare them to the corresponding experiments. One challenge is the limited quantifiable data which can be obtained from HVI experiments. The extremely short time scale and limited instrumentation mean that often high-speed photographs are the only data available from the experiments. This restricts the quantitative comparison possible between our proposed numerical model and experiments. Nevertheless, a comparison is performed from the data that are available.

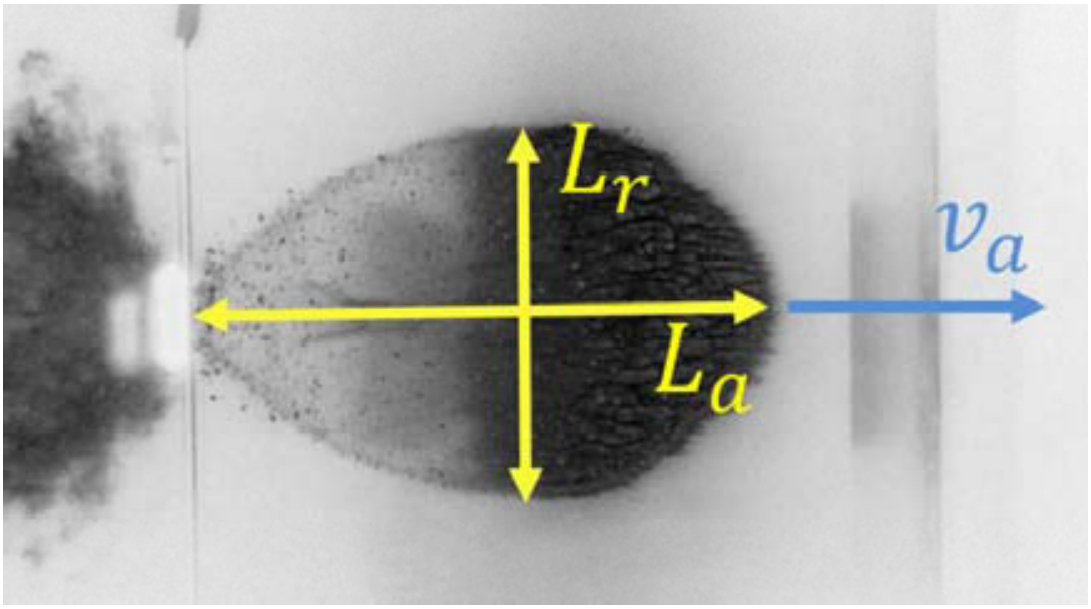

Fig. 3. Experimental high-speed photograph of the debris cloud showing the cloud's length ratio $R = L_a/L_r$, and axial expansion velocity v_a.

3.2 Extension of the Debris Cloud

One of the measurable quantities from the experiments is the debris cloud's expansion velocity. Normalizing the expansion velocities with the impact velocity, v_a / v_0 allows us to meaningfully compare cloud characteristics even at different impact velocities. In Fig. 4, we compare the calculated debris cloud's axial expansion velocity with experimental values performed by Piekutowski [6] at an impact velocity of 6.7 kms^{-1} with varying *t/D* ratio. The diameter of the impacting sphere was 9.53 mm in the simulation and experiment. At larger *t/D* ratios, the simulation model had to be rescaled to avoid simulating an unreasonable number of particles as the plate thickness increased. The dotted line represents linearly extrapolated experimental data.

In Fig. 4, the simulation over-predicts the expansion velocities, but still captures the overall decreasing trend. This decreasing trend is due to the increase in thickness of the target plate at higher *t/D* ratios. Since the sphere's size remains constant, a thicker plate requires more momentum to be transferred from the impactor particles to the plate particles. This increases the total mass in the debris cloud, but reduces its velocity. The simulations' over-prediction of expansion velocities, as seen in Fig. 4, result from the lack of a dissipative energy term in our model. Physically speaking, the passing of a shock wave is a highly transient process during which some of the kinetic energy is converted into heat as the material behind a shock wave experiences a sudden jump in thermodynamic variables such as pressure, energy, and density. This jump between two points of the Hugoniot curve takes place along the Rayleigh line and is a highly non-isentropic process. The rarefaction waves that bring the material back to ambient condition occur on an isentropic path. The difference in entropy gained in the process is therefore converted into heat which is absorbed by the material. If the shock pressure is high enough, melting or vaporization will occur.

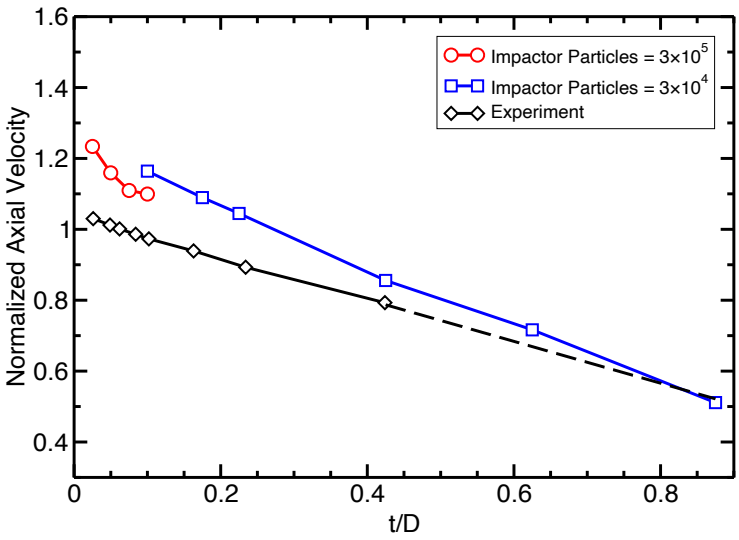

Fig. 4. Debris cloud axial expansion velocity with v_0 = 6:7 km/s at different t/D ratios. The simulation results are compared to experiments by Piekutowski [6]. The dotted line represents linearly extrapolated experimental data.

Without any dissipative effects in the model to account for heating and melting, all of the energy from the passing shock wave, except what is lost within the broken bonds, is recovered and transformed into kinetic and potential energy. This results in too much kinetic energy assigned to certain particles, leading to an overestimate of the cloud expansion velocity when compared to the experiment. A secondary effect of the lack of energy dissipation is a more diffuse boundary in the simulation debris cloud caused by a large variation in particle velocities. In contrast, the heating and melting in the experiment limit the particle velocities and help to create a sharper cloud boundary, as can be seen in Fig. 5.

3.3 Shape and Degree of Fragments

Although the expansion velocities of the debris cloud provide useful and easily quantifiable information, they do not completely characterize the debris cloud; namely, the shape and degree of fragmentation of the cloud is not accounted for. Unfortunately, experiments do not generally provide a quantitative analysis of the fragmentation of the debris cloud distribution, so one usually depends on visual inspection. We provide such a visual comparison in Figs. 5 and 6, which show simulation and experimental snapshots of the debris clouds resulting from the impact of an aluminum sphere on plates of different thicknesses at v_0 = 6.7 km/s. When the equivalent simulation and experiments are compared, it becomes apparent that the shape and degree of fragmentation play an important role in the debris cloud characterization. In Fig. 7 we display as an example a histogram of the mass distribution for the case of a cylinder impact on a plate at 5.7 km/s, which reveals one intact fragment and thousands of small fragments in the debris cloud.

Similarities in debris cloud shape and fragmentation level can be seen in Fig. 6 showing impacts with high *t/D* ratios, but strong differences in shape and fragmentation occur at the low *t/D* ratio range. Figure 7 compares the experiment and simulation debris cloud resulting from an impact with *t/D* = 0.05, which exhibit very noticeable differences such as:

- The well-defined frontend (left side of debris cloud) as seen in the experiment is missing in the simulation.
- The large central fragment in the simulation did not fracture into a distinctive debris bubble behind the dense cloud center (right side of debris cloud) as seen in the experiment.

The lack of a well-defined frontend structure is due to the absence of dissipative mechanisms in our simple model to account for heating and melting as previously explained. The failure to form a distinctive debris bubble at the rear of the cloud results from the model's limitation when the shock pressures are too low. The amplitude of a shock wave in HVI is dependent on the impact velocity and the combined geometry of target and impactor.

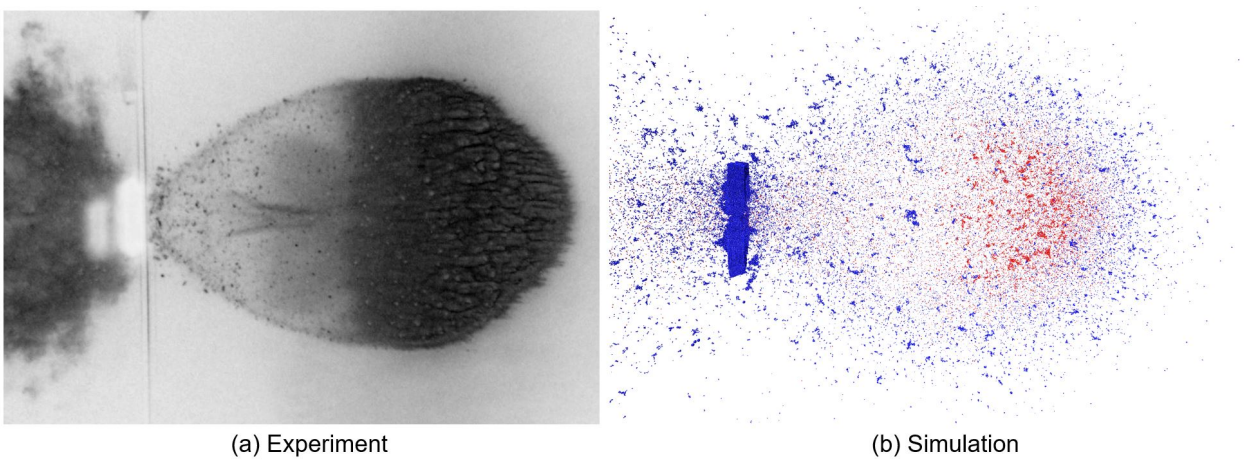

Fig. 5. Comparison of experiment and simulation of HVI of an aluminum sphere on an aluminum plate at 6.5 km/s.

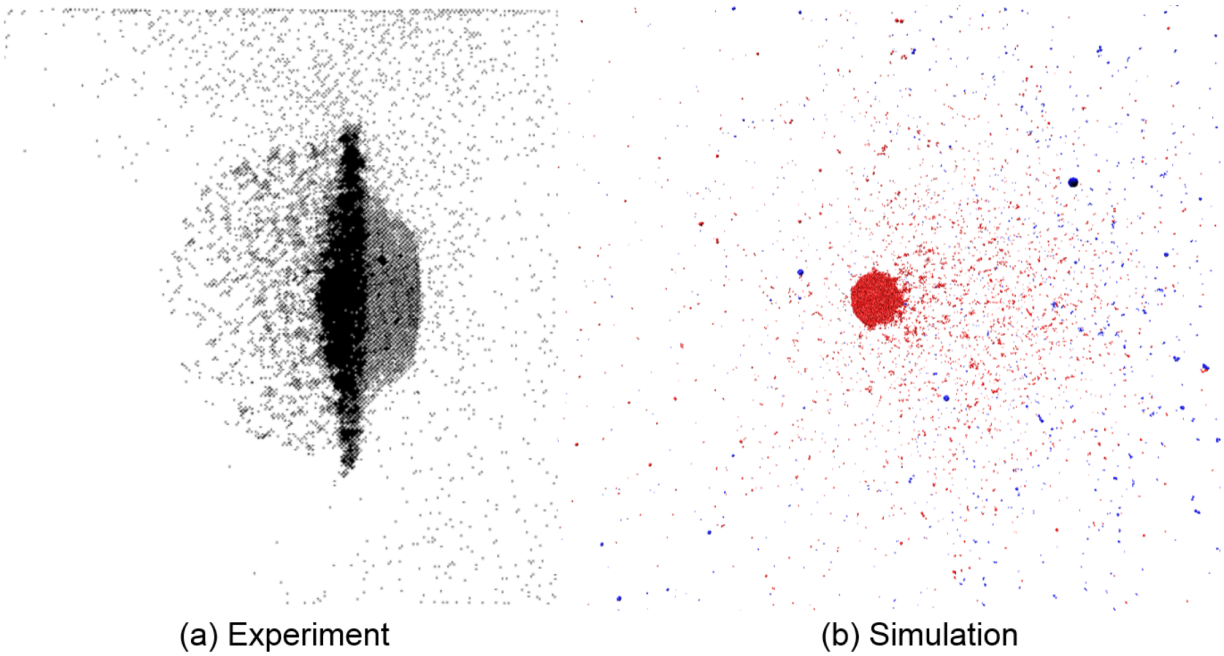

Fig. 6. The shape of the debris cloud is highly affected by the *t/D* ratio. (a) High-speed radiograph of experiment; (b) 3D simulation with v_0 = 6.7 km/s and *t/D*=0.05. The simulation performs poorly at extremely small *t/D* ratios, but very well at large values, cf. Fig. 4. Experimental snapshot from Piekutowski [6].

Upon impact, two shock waves form and propagate away from the interface between the plate and impacting sphere. When these shock wave reach the free back end of the plate or impacting sphere they are reflected as rarefaction waves, which are tensile waves. If the net tensile stress due to any rarefaction wave exceeds the fracture stress of the material, spallation will occur.

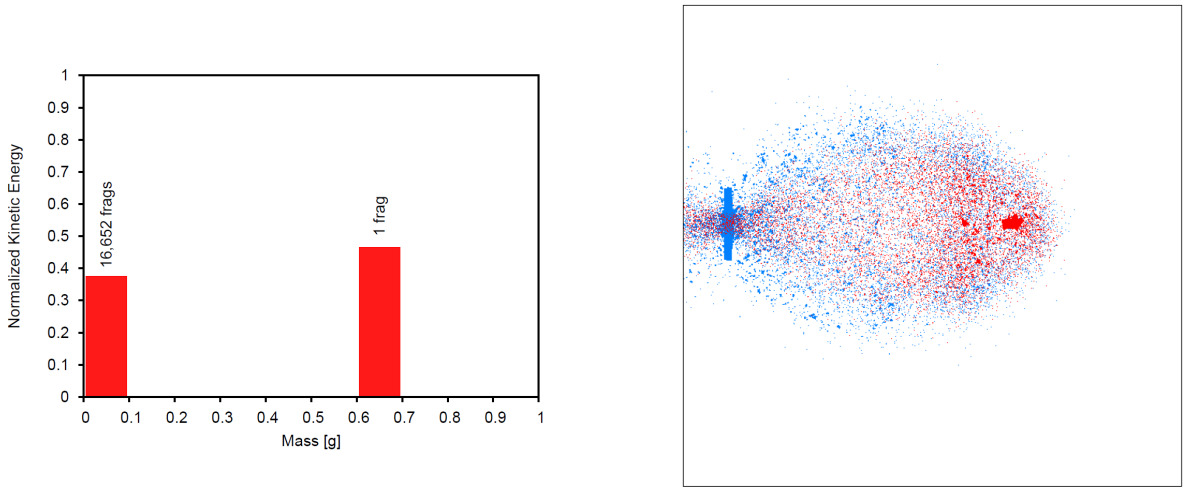

Fig. 7. HVI simulation of a cylinder impact on thin plate. Histogram of the mass distribution in the debris cloud.

Because rarefaction waves propagate faster than shock waves, at small ratios of plate thickness to projectile length, i.e., the *t/D* ratio, the rarefaction wave reflected off the target plate may overtake and attenuate the shock wave in the projectile. Therefore, in HVI with a low *t/D* ratio, the impactor may only experience a weakened compressive wave. In such cases, the remaining amplitude of the compressive and tensile stresses in the impactor may no longer be many times higher than the material's shear and tensile strength. In such a case, our original assumption of material strength playing a very small role in the overall system behavior no longer holds true and the model ceases to yield accurate results.

4 REFERENCES

1. Steinhauser, M.O. *Computer Simulation in Physics and Engineering*, deGruyter, Berlin, Germany, Boston, MA, USA, 2013.
2. Steinhauser, M.O. *Computational Multiscale Modeling of Fluids and Solids*, 2nd ed., Springer, Berlin/Heidelberg, Germany, 2017.
3. Kadau, D., Bartels, G., Brendel, L., Wolf, D.E. Contact dynamics simulations of compacting cohesive granular systems, Comp. Phys. Commun. Vol. 147, pp. 190–193, 2002.
4. Leszczynski, J.S. A discrete model of a two-particle contact applied to cohesive granular materials, Granul. Mat. Vol 5, pp. 91–98, 2002.
5. Jones, J. E. On the determination of molecular fields. I. From the variation of the viscosity of a gas with temperature, Proc. R. Soc. A Math. Phys. Eng. Sci., Vol. 106, pp. 441–462, 1924.
6. Piekutowski, A.J. Formation and Description of Debris Clouds Produced by Hypervelocity Impact, Technical Report NASA Contractor Report 4707; University of Dayton Research Institute: Dayton, OH, USA, 1996.

5 CONCLUSIONS

In this paper, we explore the suitability of simulating impacts at velocities beyond 5 km/s with DEM simulations. We propose a very simple model with three free parameters using two cohesive and repulsive potentials. In developing the model, we postulated that the extremely high pressures experienced by the material under HVI would relegate its material strength to a minor role. We assume that the material under impact behaves like a viscous fluid instead of a rigid solid, hence allowing a simplified model.

The model's parameters are determined by comparing the simulation results to experimental data taken from literature and performed at the Fraunhofer Ernst-Mach- Institute's hypervelocity testing facility. When evaluating

the model's suitability, we find good correspondence between simulation and experiment when the impact conditions lead to strong shock waves propagating through the material, but poor results when the impact velocity or geometry hinders strong shocks from forming. We present here a comprehensive parameter study to evaluate the model's range of validity, in terms of impact velocity and geometry.

In a follow-up study currently underway, we are extending our model to account for dissipative effects such as heating and melting. We plan to investigate more complex and comprehensive models that will lead to accurate simulations at low shock pressures. We are also expanding the model to new impact geometries such as Whipple shields used for spacecraft shielding and to different impactor geometries such as cylinders. We plan to analyze the debris cloud resulting from such impacts with respect to fragment size, kinetic energy, cloud shape, and expansion velocity.